δ TRIP steel

S. Chatterjee, M. Murugananth and H. K. D. H. Bhadeshia*

A combination of neural networks and genetic algorithms has been used to design a TRIP assisted steel in which the silicon concentration is kept low. In this context, the steel has a novel microstructure consisting of δ ferrite dendrites and a residual phase which at high temperatures is austenite. This austenite can, with appropriate heat treatment, evolve into a mixture of bainitic ferrite and carbon enriched retained austenite. The steel has been manufactured and tested to reveal a tensile strength of $\sim$1 GPa and a uniform elongation of 23%.

Keywords: TRIP assisted steel, Martensite, Bainite, δ Ferrite

Introduction

Steels, the mechanical properties of which are assisted by transformation induced plasticity and yet, do not contain expensive alloying elements, are now well established. These so called TRIP assisted steels have a microstructure dominated by allotriomorphic ferrite. However, a substantial minority of the microstructure consists of bainitic ferrite and retained austenite. It is the latter which can be induced to transform into martensite during deformation.[1–10]

The critical solute in TRIP assisted steels is silicon, which at a concentration of $\sim$1·5 wt-%, prevents the precipitation of cementite during the growth of bainitic ferrite.[11] As a consequence, the carbon that partitions into the residual austenite stays there, allowing the austenite to be retained to ambient temperature.

This relatively large concentration of silicon can cause the formation of an adherent surface scale which makes the steel unsuitable for applications where the cosmetic appearance is important.[12,13] The aim of the present work was to create and validate a mathematical framework which allows the following question to be posed: what is the combination of alloying elements and processing which can lead to an optimum quantity of retained austenite in the microstructure and yet minimise the silicon concentration?

In attempting to answer this question, the model assembled led to a novel concept for TRIP assisted steels. The present paper begins with a description of the model, followed by the experiments conducted to validate the prediction made.

Network relating composition, processing and structure

In the present context, the optimisation process needs access to a quantitative relationship between the chemical composition of the steel, the heat treatment and the ultimate microstructure (in this case, the quantity of retained austenite). A neural network method was used for this purpose. The particular method used has been extensively described previously.[14–17] Its applications have also been widely published[18–28] and hence, only the salient points are reproduced here.

The neural network is a non-linear regression method which can capture enormous complexity in the data, while avoiding overfitting. The Bayesian framework of the network used in the present work is able to indicate two uncertainties. The first is the *noise* in the output when an experiment is not exactly reproducible because some variables are not controlled. The noise is usually expressed as a constant number. The second is the *uncertainty of modelling* because many mathematical functions are able to fit the same data, which however, behave differently when extrapolated. This latter uncertainty is important in identifying domains where care must be exercised in interpreting the results from a network. The modelling uncertainty is also helpful in identifying regions of the input space where data are sparse. The magnitude of the modelling uncertainty varies with the position in the input domain where calculations are conducted.

The data used to create the model were compiled entirely from published sources[2,6–8,29–41] to include the variables listed in Table 1.

Owing to a lack of data, it was impossible to include the heating rate to the intercritical annealing temperature as a variable. Its effect would therefore be included in the noise: the exact contribution cannot be estimated but it must be less than the total noise which was $\pm$4% in the trained models. Predictions were made using the neural network model by varying input variables over a base steel composition of 0·2C–1·5Mn–1·0Si–0·5Al–0·02P–0Mo–0Cu (wt-%), intercritical annealing parameters of 780°C for 300 s and bainite transformation conditions as 400°C for 500 s.

Some examples of trends perceived by the trained neural network model are illustrated in Fig. 1. It is interesting that both silicon and aluminium help retain austenite, not by increasing its thermodynamic stability but rather by stopping the precipitation of cementite during the bainite reaction. The trends are as expected

Materials Science and Metallurgy, University of Cambridge, Pembroke Street, Cambridge CB2 3QZ, UK

*Corresponding author, email hkdb@cam.ac.uk

Published by Maney on behalf of the Institute
Received 19 November 2006; accepted 25 January 2007
DOI 10.1179/174328407X179746

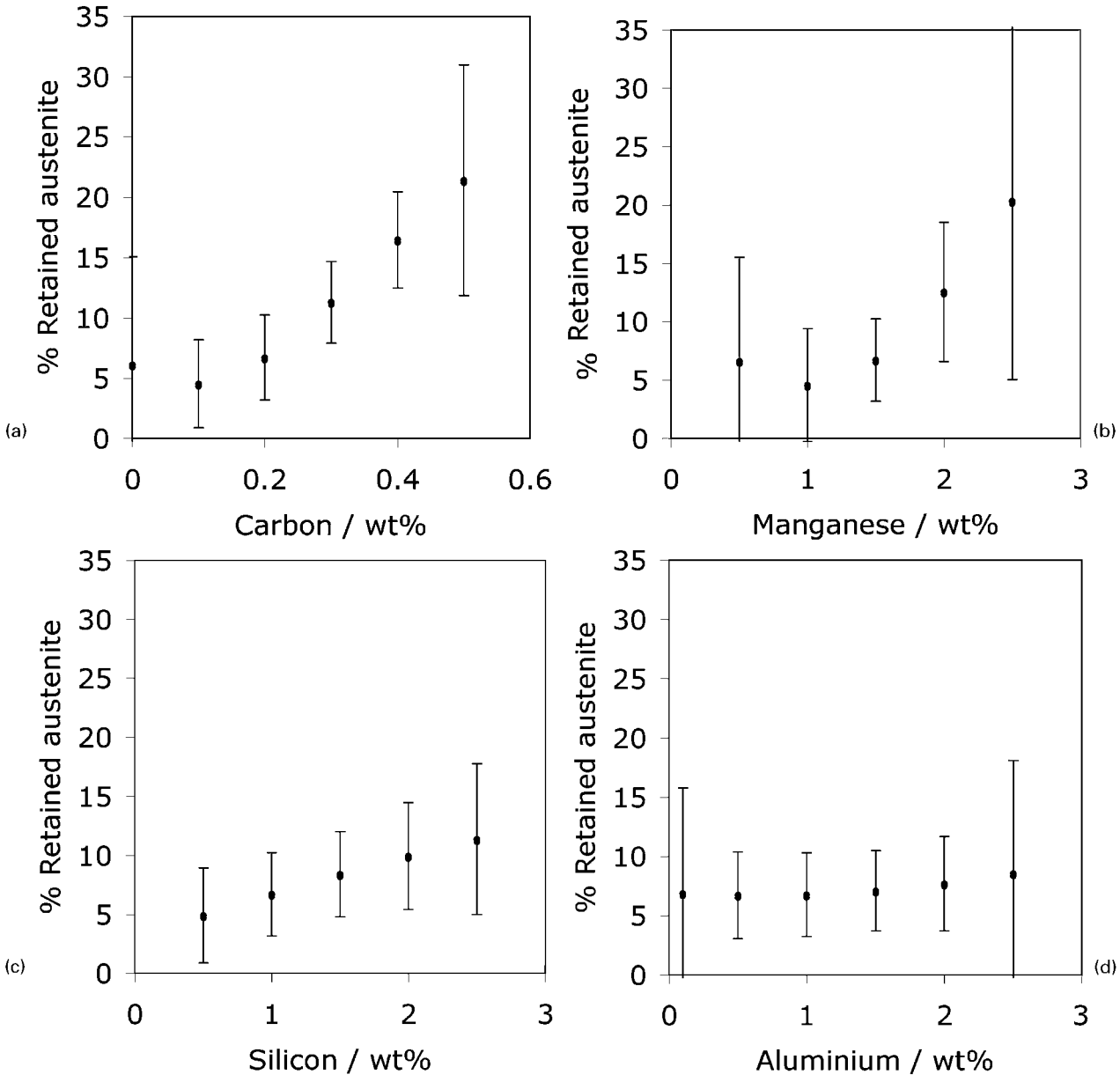

a carbon; *b* manganese; *c* silicon; *d* aluminium

1 Effect of alloying elements on retained austenite fraction: error bars represent $\pm 1\sigma$ modelling uncertainties; noise by contrast, not plotted here, is a constant $\pm 1\%$ of retained austenite

from a metallurgical point of view: those due to heat treatments are illustrated in Fig. 2. The retained austenite content goes through a minimum as a function of the intercritical annealing temperature T_{IC}. This is because the equilibrium carbon concentration of austenite increases as T_{IC} decreases, whereas substitutional

Table 1 Data used for modelling retained austenite fraction*

Variable	Minimum	Maximum	Average	σ
Carbon, wt-%	0·0950	0·3920	0·2102	0·1020
Manganese, wt-%	0·6000	1·9900	1·4057	0·2796
Silicon, wt-%	0·0400	2·1000	0·9619	0·5369
Aluminium, wt-%	0·0000	2·0000	0·2979	0·5236
Phosphorus, wt-%	0·0000	0·2040	0·0223	0·0401
Molybdenum, wt-%	0·0000	0·1400	0·0043	0·0218
Copper, wt-%	0·0000	0·5100	0·0065	0·0573
IA temperature, °C	730	840	778·2653	25·7829
IA time, s	60	450	213·2143	110·8414
IT temperature, °C	300	525	404·2347	39·5554
IT time, s	0	5400	441·3673	588·7228
Retained austenite, vol.-%	0·12	27·07	10·3805	5·8054

*IA, intercritical annealing; IT, isothermal transformation to bainite; σ, standard deviation.

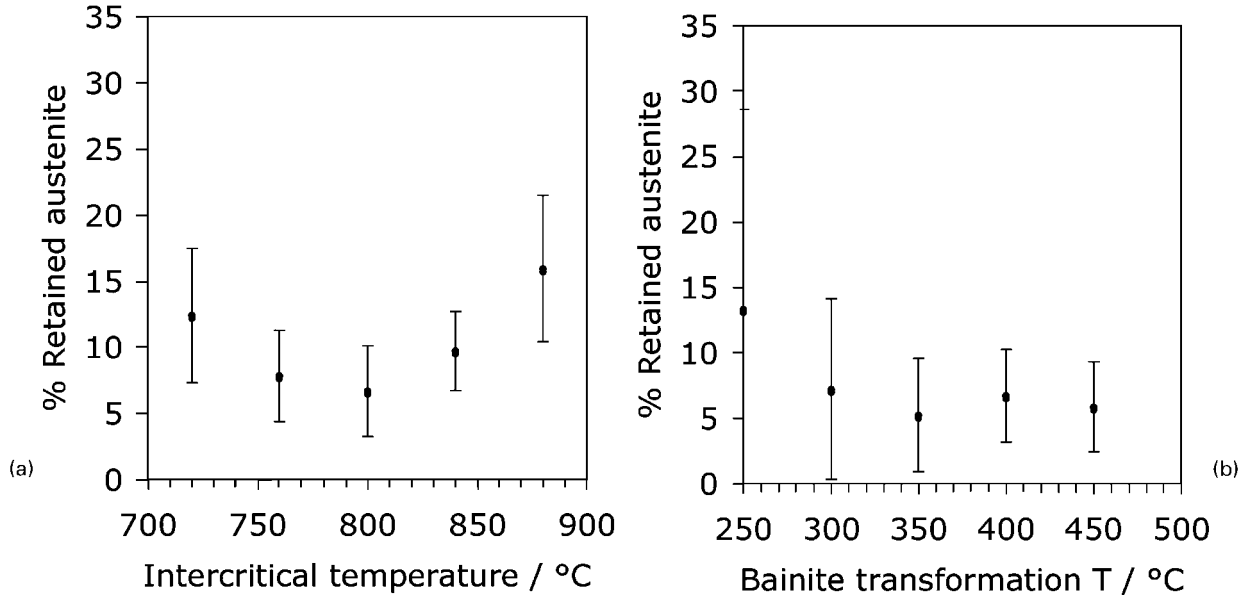

a intercritical annealing temperature; *b* bainite transformation temperature

2 Effect of heat treatment parameters on retained austenite fraction: error bars represent $\pm 1\sigma$ modelling uncertainties

solute partitioning during austenitisation enhances the stability of the austenite at high T_{IC}. The trend as a function of the bainite reaction temperature is just perceptible, but can be understood in that the limiting carbon concentration of the austenite is greater at lower temperatures.[11]

Many such trends were examined but are not reported here for the sake of brevity; details can be found in a recent thesis.[42] Suffice it to say that the model seems to predict reasonable trends relating the retained austenite fraction with the input variables. The model has also been made freely available.[43] It was then used to formulate an optimum chemical composition of these materials, as described in the next section.

Optimisation

Design problems usually begin with specification of a target. Neural network models can be interrogated with sets of inputs until the desired output is achieved. A more economical method, possibly a method capable of reaching an optimum solution, is to allow the inputs to the neural network to *evolve* towards the desired output (*see* Ref. 44). A point is chosen in the design space around which a family of points is generated by mutating the original. Recombinations, in which a few of the variables within a set are exchanged between sets, are also a part of the process. The survival of any set depends on how close it matches the desired output.

In the present work, a commercially available genetic algorithm[45] was used in combination with the neural network model to define an optimum TRIP assisted steel in which the retained austenite content is maximised while keeping the silicon concentration to a minimum. This procedure on its own may not ensure a good TRIP steel but is about the austenite–silicon relationship. Concentrations of all the other solutes with the exception of phosphorus were allowed to vary, as were the heat treatment temperatures. However, the heat treatment times at these temperatures was kept constant to fit with commercial requirements at 60 s for intercritical annealing and 900 s for transformation to bainite. A constraint was placed on the modelling uncertainty such that input sets which led to this uncertainty exceeding $\pm 20\%$ of the desired value of the output were rejected.

The algorithm converged to an alloy with the chemical composition Fe–0·4C–2Mn–0·5Si–2Al–0·5Cu–0·02P (wt-%), with a microstructure estimated to contain 41 ± 20 vol.-% of retained austenite, after intercritical annealing at 840°C (60 s) followed by bainite transformation at 300°C (900 s). Perhaps not surprisingly, the alloy is rich in carbon, manganese, aluminium and copper. It is odd that the algorithm maintained the silicon at 0·5 wt-% rather than zero, in spite of the large aluminium concentration which should be sufficient to suppress cementite precipitation from austenite. The reason for this is not clear. Copper of course is a useful element to stabilise the austenite and phosphorus has the ability to retard cementite.

Thermodynamic analysis

The fractions and compositions of the equilibrium phases of the alloy were estimated using MT-DATA[46] with the SGTE database. The calculations were conducted allowing ferrite, austenite, cementite and liquid to exist. The results are presented in Fig. 3. The alloy

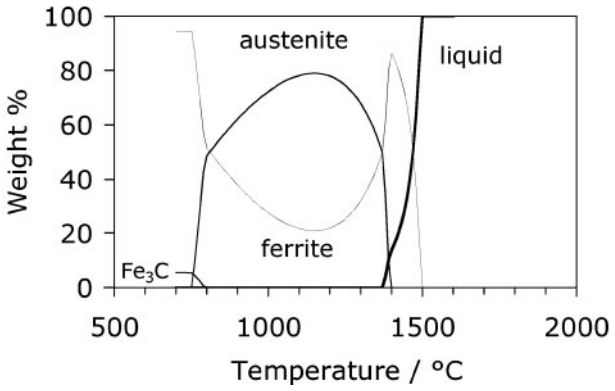

3 Calculated quantities of phases as function of temperature for optimised alloy

starts to solidify by forming δ ferrite, which reaches a maximum of $\sim$85 wt-%. Some of the δ ferrite then transforms into austenite during cooling, although the alloy never becomes fully austenitic. The maximum predicted amount of austenite is $\sim$80 wt-%, some of which transforms back into α ferrite on continued cooling. Note that δ and α ferrites are identical in crystal structure: the terminology does however help distinguish the δ ferrite which forms as dendrites during the solidification of liquid and the α ferrite which occurs by the solid state transformation of austenite. The results indicate that dendrites of δ ferrite should remain in the sample cooled to ambient temperature.

At 840°C, the alloy is predicted to contain $\sim$54 wt-% austenite and 46 wt-% ferrite. The chemical composition of the austenite at that temperature is Fe–0·67C–2·54Mn–0·53Si–1·35Al–0·013P–0·51Cu (wt-%). It is of interest to examine the formation of bainite and martensite in austenite of that composition. These calculations were carried out using the method described in Refs. 47–50. The method is available freely and is designated MUCG73 on the Materials Algorithms Library.[43] In this way, the bainite and martensite start temperatures of the austenite at 840°C were calculated to be 354 and 160°C respectively. Both the predicted intercritical annealing and the bainite reaction temperature of 300°C therefore appear reasonable.

The carbon concentration of the austenite x_γ at the point where the bainite reaction would cease at 300°C can be calculated from the fact that diffusionless transformation is impossible once x_γ equals the x_{T_0} given by the T_0 curve on the phase diagram.[11] The latter was calculated using MUCG73 to be 1·115 wt-% (0·0497 mole fraction) for austenite formed during intercritical annealing at 840°C and transformed at 300°C. Using mass balance, this means that only 34 wt-% of the original 54 wt-% of the austenite remains untransformed after the formation of bainite. Because this residual austenite has a very high carbon concentration, it is fully retained to ambient temperature since its calculated martensite start temperature is below ambient temperature at −27°C. The 34 wt-% of retained austenite calculated in this way is in good agreement with the predictions made using the neural network and genetic algorithm at roughly 40 ± 20 wt-%.

Aluminium is known to be a γ loop forming element and its presence in a concentration as large as 2 wt-% is probably the key factor preventing a fully austenitic state from being achieved. The view was taken that TRIP assisted steels in any case contain a large quantity of ferrite apart from the minority constituents of bainitic ferrite and retained austenite. It would be reasonable to consider the same concept as conventional TRIP assisted steels but with the allotriomorphic ferrite replaced by δ ferrite. Experiments were therefore undertaken to investigate the concept further.

Experimental details

The initial work was done on a small 50 g melt made in an electric arc furnace at Cambridge University, designated 'A' in Table 2. The remaining alloys were made as 50 kg melts in an air melting furnace at Tata Steel (India). For optical microscopy, the samples were prepared using standard metallographical techniques and etched using 2% nital solution. Higher resolution observations were done using field emission gun scanning electron microscopy (FEGSEM) operated at a 10 kV accelerating voltage.

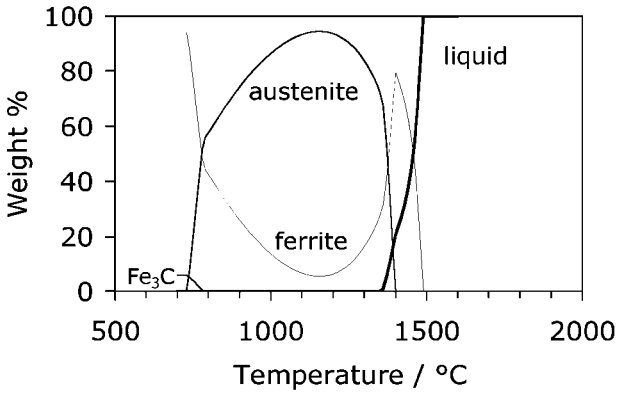

4 Calculated equilibrium phase constitution of alloy A

X-ray diffraction tests of the samples were carried out with a scan range of 40–120° at 0·5° intervals and a 5 s dwell at each step. Cu K_α radiation was used and the operating voltage and current were set at 40 kV and 40 mA respectively. Retained austenite measurements were done on metallographically prepared samples etched with 2% nital solution and then once again fine polished. X-ray data were analysed using the X'Pert Plus software which uses the Reitveld refinement method due to Wiles and Young.[51]

Bulk Vickers hardness and the microhardness were recorded using 10 kg and 50 g loads respectively.

Uniaxial tensile tests on samples of 5 mm diameter and 30 mm gauge length were carried out both at room temperature and at 100°C at a strain rate of $2{\cdot}8 \times 10^{-5}$ s^{-1}. An extensometer of 10 mm gauge length was attached to the specimen tested at room temperature but this was impossible for the higher test temperature. Samples cut $\sim$1 mm from the broken surfaces were used for X-ray diffraction studies to measure the fraction of austenite remaining at fracture.

All heat treatments were carried out with the samples sealed in quartz tubes containing a partial pressure of argon.

Cast microstructure

Although alloy A deviates from the intended composition (Table 2), it nevertheless has a similar phase constitution as illustrated in Fig. 4, with δ ferrite being incompletely transformed as the alloy cools to ambient temperature.

The microstructure in the as cast condition is consistent with the phase diagram calculations. Figure 5 shows the light etching dendrites of δ ferrite. The darker regions represent the austenite which existed at elevated temperatures but has transformed into a fine microstructure on cooling. The micrograph also reveals a dark

Table 2 Chemical composition of model perceived optimum alloy and experimental alloys, wt-%

Alloy	C	Mn	Si	Al	P	Cu
Optimum	0·40	2·00	0·50	2·00	0·02	0·50
A (small casting)	0·41	2·42	0·46	1·57	0·26	0·42
B (large casting)	0·36	1·96	0·73	2·22	0·022	0·52

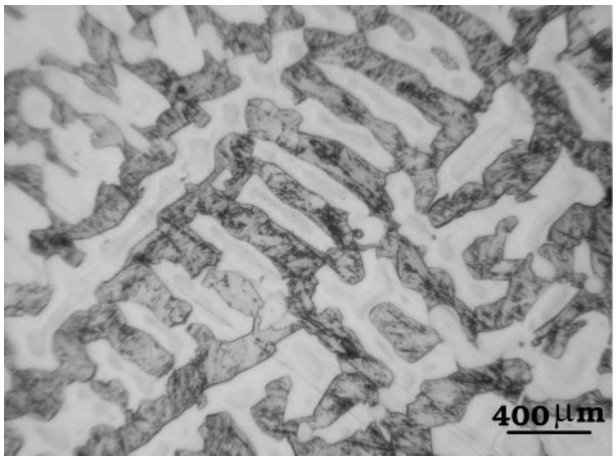

5 Optical micrograph of alloy A in as cast condition

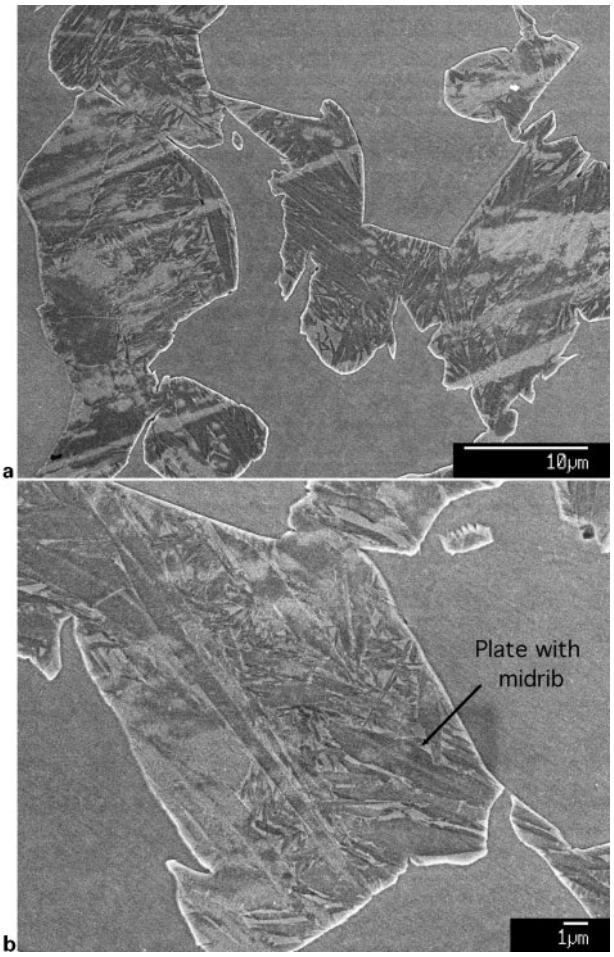

6 FEGSEM images revealing martensite-like plates in residual phase of as cast alloy A: higher magnification image (*b*) reveals midribs in some of plates

etching residual phase, the nature of which is not clear from Fig. 5. The higher resolution images in Fig. 6 indicate that the austenite in the as cast alloy has transformed into martensite plates. Some of the plates are seen to contain midribs, which are consistent with a transformation twinned region.[52] The morphological observations therefore suggest high carbon plate martensite.

The hardness of the δ ferrite and the darker etching region in the as cast microstructure in Table 3 is consistent with the latter region containing a substantial amount of high carbon martensite. The hardness data were used to estimate the volume fractions of the constituent phases in the as cast sample using a rule of mixtures. If H_1 and H_2 are the microhardnesses of δ ferrite and the residual phase respectively, and if it is assumed that the bulk hardness H_b of the sample can be written

$$H_b = vH_1 + (1-v)H_2 \quad (1)$$

then v, the volume fraction of δ-ferrite, can be estimated. A point count method was also used to measure the phase fractions. Assuming that the densities of the two phases are not significantly different, the measurements effectively represent the weight fraction of each phase, as presented in Table 3.

A comparison of the measured fractions against Fig. 4 indicates that during cooling, the δ ferrite fraction did not change once a temperature of 1400°C was reached. For that temperature, the calculated[46] phase compositions are given in Table 4. The liquid coexisting with the δ ferrite at 1400°C is rich in carbon (Table 4). This liquid becomes austenite on solidification, thus explaining the large hardness of the martensite. However, some austenite must also remain untransformed, due to its high carbon content. X-ray diffraction showed that about 7·8±0·7 wt-% of retained austenite is present in the sample in the as cast microstructure.

A set of as cast samples of the alloy was tempered at 300°C for a variety of time periods, to confirm the carbon content of the martensite. As expected, the microhardness of the phase was found to decrease dramatically with increasing tempering time (Table 5).

Table 4 Calculated amount and chemical composition of phases in equilibrium for alloy A at 1400°C

		Composition, wt-%					
Phase	Amount, wt-%	C	Mn	Si	Al	P	Cu
Ferrite	79·5	0·2	2·1	0·4	1·7	0·2	0·4
Liquid	20·5	1·2	3·7	0·7	1	0·2	0·4

Table 3 Weight fraction and microhardness of constituent phases in as cast microstructure*

		Weight fraction	
Phase	Vickers hardness, HV	From hardness	From point count
δ Ferrite	296±20	0·77	0·74±0·04
Residual phase	801±57	0·23	0·26±0·01
Bulk	412±25		

*Errors represent $\pm 1\sigma$. The bulk macrohardness is also stated. Each hardness value is an average of 20 measurements.

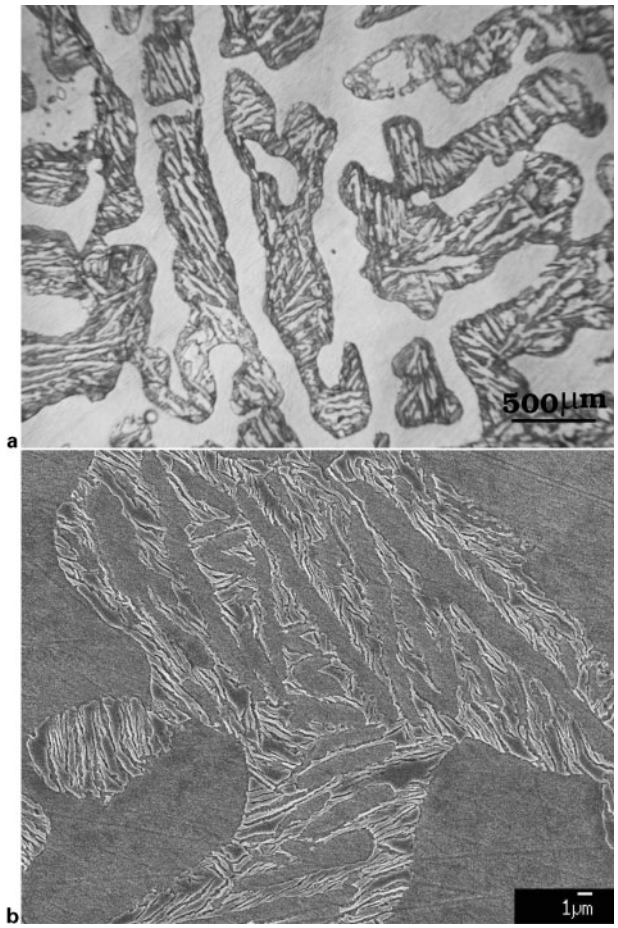

a optical micrograph; *b* FEGSEM image

7 Alloy A heat treated to produce bainite

Production of bainite

The residual austenite in the as cast microstructure transformed on cooling to martensite, leaving little retained austenite. TRIP assisted steels rely on it transforming into bainitic ferrite to leave carbon enriched retained austenite.

In industrial practice, TRIP assisted steels are induced to transform into bainite either by coiling the steel at a high temperature or by arranging the cooling conditions such that the steel spends time within the bainite transformation range. To simulate this, samples of alloy A were first heated to 810°C where ~60 wt-% of austenite is expected at equilibrium (Fig. 4). After 12 h at 810°C, the samples were transformed isothermally at 300°C for 6 h. The choice of this time was made by calculating the transformation kinetics for the expected composition of the austenite, using the method described in Ref. 50.

Figure 7 shows the mixture of bainitic ferrite and austenite obtained, together with the dendrites of δ ferrite. X-ray analysis revealed 14·3±0·7 wt-% retained austenite and its carbon content was deduced to be 1·35±0·02 wt-% from the lattice parameter using an equation due to Dyson and Holmes.[53] The quantity of austenite is however less than the mean value expected using the model, which for alloy A is predicted to be 39±30%.

Table 5 Decrease in microhardness as martensite tempers at 300°C

Tempering time, h	Microhardness, HV
0	801±57
1	655±23
2	606±30
4	529±36

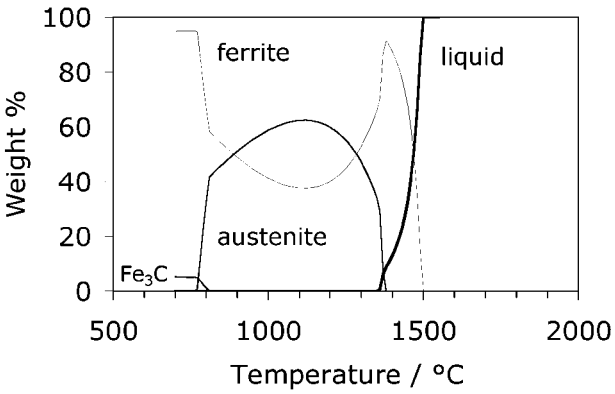

8 Phase constitution for alloy B, calculated using MT-DATA

Large casting

As expected from Fig. 8, the microstructure of the alloy in the as cast condition reveals δ ferrite dendrites (microhardness 214±8 HV) and a dark etching residual phase with a microhardness of 382±22 HV (Fig. 9*a*). The latter turned out to pearlite instead of martensite, presumably because of the slower cooling rates associated with a large casting (Fig. 9*b*).

Figure 8 shows that alloy B consists of 45 wt-% ferrite and 55 wt-% austenite in equilibrium at 940°C. Samples were therefore heated at 940°C for 12 h and then allowed to transform into bainite at 300°C for 3 h.

Figure 10 shows that the distinct morphology of the δ ferrite is retained after the heat treatment, although some austenite has grown into the former δ ferrite. Bainite has also been induced into the remaining microstructure and X-ray diffraction analysis revealed 13·5± 0·9 wt-% retained austenite containing about 1·17± 0·03 wt-% carbon.

The microhardnesses of δ ferrite and bainite along with the bulk hardness of the heat treated sample are presented in Table 6. The data in Table 6 show that the observed phase fractions are consistent with the calculated phase constitution (Fig. 8).

Heat treated samples of the alloy B were tensile tested. The properties observed at room temperature exhibit a 23% total elongation and an ultimate tensile strength of 1000 MPa (Fig. 11). The 0·2% proof stress was recorded as 700 MPa. No significant necking of the sample at fracture occurs with almost all the observed elongation being uniform. Figure 12 shows the data for the δ TRIP steel plotted against a large amount of information from the literature for a variety of TRIP assisted steels. Point 'A' is plotted following the strict definition of uniform elongation whereas point 'B' represents the total elongation, bearing in mind that the elongation to failure is almost entirely uniform. It is seen that the properties of the δ TRIP steel are impressive.

The true stress–strain plot in Fig. 11 shows steady strain hardening continuing until fracture, attributed to the transformation of retained austenite into martensite

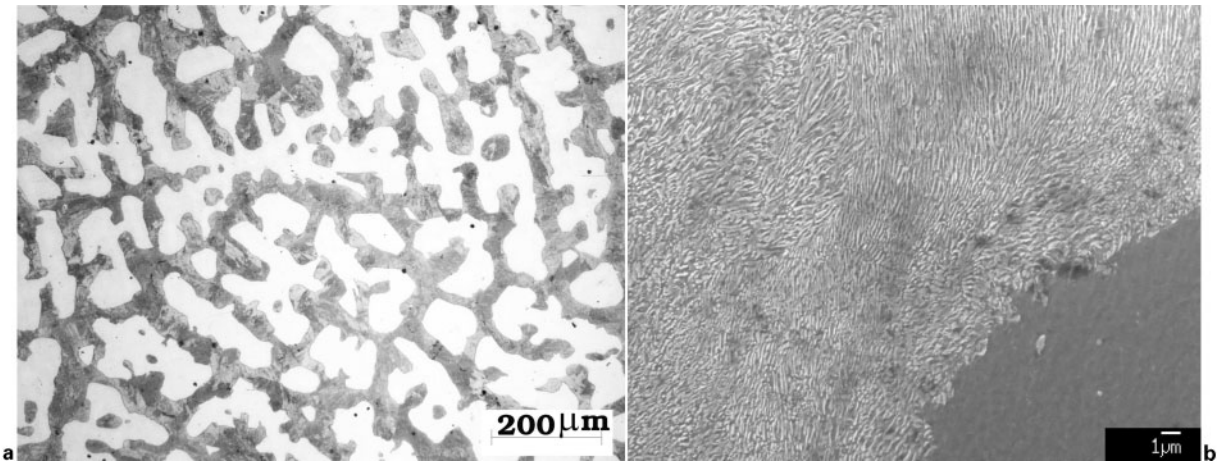

a optical micrograph; *b* FEGSEM image

9 Microstructures of as cast alloy B

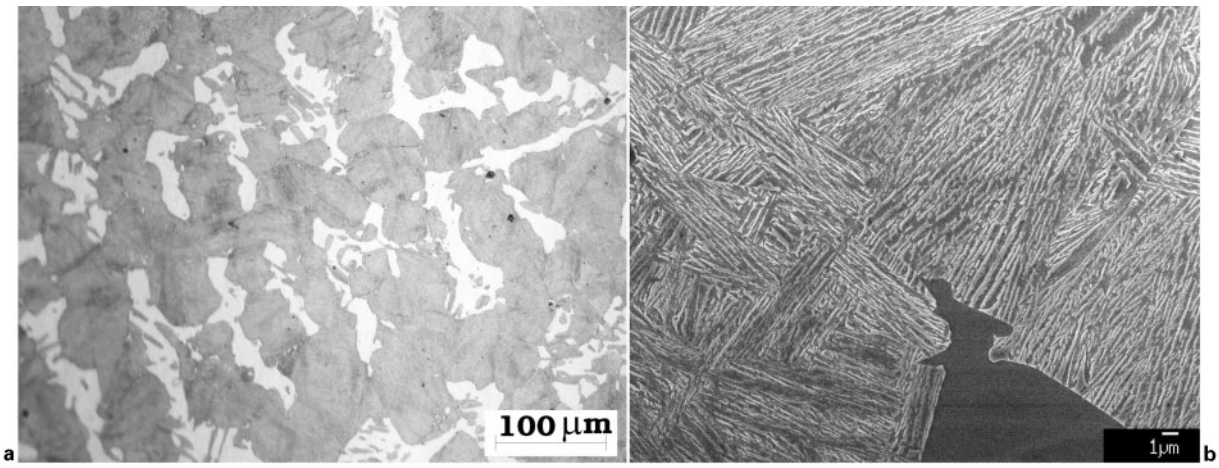

a optical micrograph; *b* FEGSEM image

10 Microstructures of heat treated sample

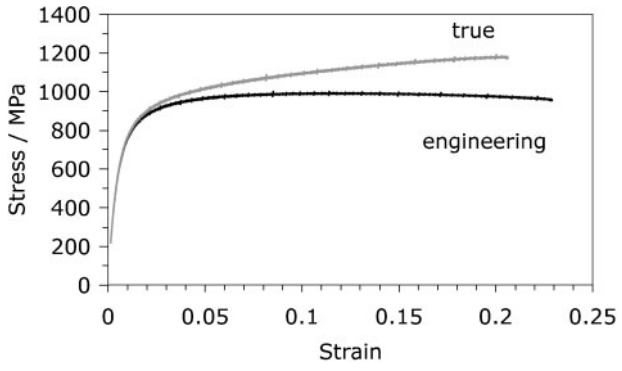

11 Stress–strain curve of heat treated material at room temperature: almost all elongation is uniform

during deformation. The X-ray analysis of a sample cut from near the fracture surface of the tensile specimen indicated that $7{\cdot}0 \pm 0{\cdot}8$ wt-% of austenite exists, a reduction by a factor of ~ 2 relative to the undeformed state. Bhadeshia[54] has indicated that in a bainitic microstructure, the austenite loses percolation when its quantity decreases below $\sim 10\%$ of the microstructure. This is approximately consistent with the fact that fracture has occurred leaving $\sim 7\%$ of retained austenite.

To test further the role of the retained austenite, a tensile test was conducted at 100°C to reduce its propensity to transform into martensite during deformation. As pointed out earlier, an extensometer could not be used so the strain is recorded from the crosshead movement. The more gradual slope of the elastic part of the curve is therefore an artefact of the method.

Table 6 Weight fraction of δ ferrite and bainite phases in heat treated sample*

		Weight fraction	
Phase	Vickers hardness, HV	From hardness	From point count
δ Ferrite	267 ± 9	0·53	$0{\cdot}43 \pm 0{\cdot}02$
Bainite	519 ± 13	0·47	$0{\cdot}57 \pm 0{\cdot}03$
Bulk	385 ± 40		

*Also included are microhardness and macrohardness values for individual phases and the bulk sample respectively.

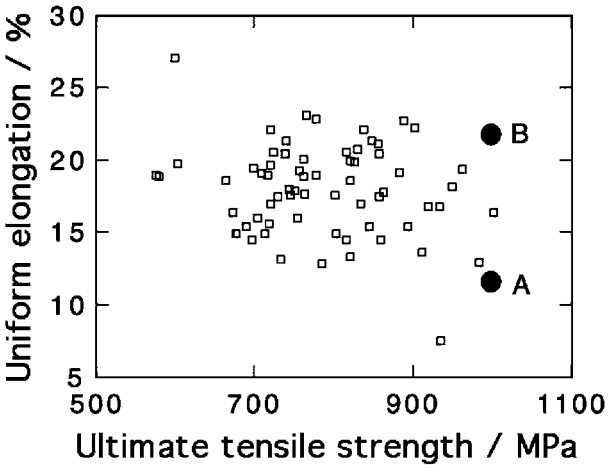

12 Comparison of properties attained against a collection of data from literature:[11] data for δ TRIP steel from Fig. 11 are plotted as black dots; point marked 'A' represents uniform elongation only and 'B' total elongation

Figure 13 shows that the strength is maintained when compared with the ambient temperature test, but the total elongation is greatly reduced, consistent with a reduction in the ability to work harden because of the increased stability of the retained austenite. Indeed, X-ray analysis confirmed that about $13{\cdot}0 \pm 0{\cdot}7$ wt-% retained austenite is present in the specimen after fracture. This is about the same as that of the heat treated state, suggesting that little strain induced transformation of austenite has occurred during straining.

Summary

Although the objective of attaining $\sim$40% of retained austenite in a TRIP assisted steel with a low silicon concentration has not been realised, the combination of neural network and genetic algorithms helped arrive at a different concept. In this, δ ferrite dendrites replace the allotriomorphic ferrite found in conventional TRIP assisted alloys.

The alloy, when transformed into a microstructure consisting of δ ferrite dendrites and a mixture of bainitic ferrite and carbon enriched retained austenite, is found to exhibit excellent tensile properties. The elongation is almost entirely uniform at $\sim$23% at ambient temperature. It has been demonstrated, by conducting an elevated temperature tensile test, that the observed elongation relies on the strain induced transformation of retained austenite into martensite.

Whether or not this design concept, designated δ TRIP steel, becomes a technological reality will depend on a variety of additional performance data. For example, the as cast steel would have to be rolled into sheet form before heat treatment into the TRIP microstructure. The authors have also not yet done any research on the important issue of weldability which would have to be considered in any serious application.

Finally, it is speculated that some of the discrepancy between the observed quantity of retained austenite and that predicted is because solidification results in a non-uniform distribution of substitutional solutes. For example, coring is evident in the δ ferrite dendrites in Fig. 5.

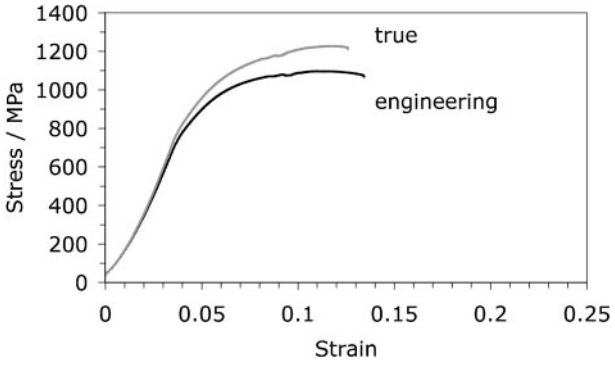

13 Stress–strain curve of material at 100°C

Acknowledgements

The authors are grateful to Tata Steel (India) for financing this work and to Professor A. L. Greer for the provision of laboratory facilities at the University of Cambridge.

References

1. O. Matsumura, Y. Sakuma and H. Takechi: *Trans. Iron Steel Inst. Jpn*, 1987, **27**, 570–579.
2. O. Matsumura, Y. Sakuma and H. Takechi: *Scr. Metall.*, 1987, **27**, 1301–1306.
3. Y. Sakuma, O. Matsumura and H. Takechi: *Metall. Mater. Trans. A*, 1991, **22A**, 489–498.
4. Y. Sakuma, O. Matsumura and O. Akisue: *ISIJ Int.*, 1991, **31**, 1348–1353.
5. Y. Sakuma, D. K. Matlock and G. Krauss: *Metall. Mater. Trans. A*, 1992, **23A**, 1221–1232.
6. Y. Sakuma, D. K. Matlock and G. Krauss: *Mater. Sci. Technol.*, 1993, **9**, 718–724.
7. M. de Meyer, D. Vanderschueren and B. C. de Cooman: *ISIJ Int.*, 1999, **39**, 813–822.
8. P. J. Jacques, E. Girault, Ph. Harlet and F. Delannay: *ISIJ Int.*, 2001, **41**, 1061–1067.
9. P. J. Jacques: *Curr. Opin. Solid State Mater. Sci.*, 2004, **8**, 259–265.
10. B. C. DeCooman: *Curr. Opin. Solid State Mater. Sci.*, 2004, **8**, 285–303.
11. H. K. D. H. Bhadeshia: 'Bainite in steels', 2nd edn; 2001, London, Institute of Materials.
12. B. Mintz: *Int. Mater.*, 2001, **46**, 169–197.
13. T. Maki and T. Furuhara: *Mater. Sci. Forum*, 2003, **426–432**, 19–26.
14. D. J. C. MacKay: *Neural Comput.*, 1992, **4**, 448–472.
15. D. J. C. MacKay: *Neural Comput.*, 1992, **4**, 415–447.
16. H. K. D. H. Bhadeshia: *ISIJ Int.*, 1999, **39**, 966–979.
17. D. J. C. MacKay: 'Information theory, inference, and learning algorithms'; 2003, Cambridge, UK, Cambridge University Press.
18. S. B. Singh, H. K. D. H. Bhadeshia, D. J. C. MacKay, H. Carey and I. Martin: *Ironmak. Steelmak.*, 1998, **25**, 355–365.
19. F. Brun, T. Yoshida, J. D. Robson, V. Narayan, H. K. D. H. Bhadeshia and D. J. C. MacKay: *Mater. Sci. Technol.*, 1999, **15**, 547–554.
20. S. Yoshitake, V. Narayan, H. Harada, H. K. D. H. Bhadeshia and D. J. C. MacKay: *ISIJ Int.*, 1998, **38**, 496–502.
21. S. H. Lalam, H. K. D. H. Bhadeshia and D. J. C. MacKay: *Sci. Technol. Weld. Join.*, 2000, **5**, 135–147.
22. S. H. Lalam, H. K. D. H. Bhadeshia and D. J. C. MacKay: *Sci. Technol. Weld. Join.*, 2000, **5**, 149–160.
23. E. A. Metzbower, J. J. DeLoach, S. H. Lalam and H. K. D. H. Bhadeshia: *Sci. Technol. Weld.*, 2001, **6**, 116–121.
24. C. Capdevila, F. G. Caballero and C. Garcia de Andrés: *ISIJ Int.*, 2002, **42**, 894–902.
25. C. Capdevila, F. G. Caballero and C. Garcia de Andrés: *Mater. Sci. Technol.*, 2003, **19**, 581–586.
26. T. Sourmail and C. Garcia-Mateo: *Comput. Mater. Sci.*, 2005, **34**, 213–218.
27. C. Capdevila, C. Garcia-Mateo, F. G. Caballero and C. Garcia: *Mater. Sci. Technol.*, 2006, **22**, 1163–1170.

28. C. Garcia-Mateo, T. Sourmail, F. G. Caballero and C. Garcia de Andrés: *Mater. Sci. Technol.*, 2005, **21**, 934–940.
29. H. C. Chen, H. Era and M. Shimizu: *Metall. Mater. Trans. A*, 1989, **20A**, 437–445.
30. Y. Sakuma, O. Matsumura and H. Takechi: *Metall. Mater. Trans. A*, 1991, **22A**, 489–498.
31. O. Matsumura, Y. Sakuma and H. Takechi: *ISIJ Int.*, 1992, **32**, 1014–1020.
32. A. Itami, M. Takahashi and K. Ushioda: *ISIJ Int.*, 1995, **35**, 1121–1127.
33. A. Pichler, P. Stiaszny, R. Potzinger, R. Tikal and E. Werner: *ISS Mech. Work. Steel Process. Proc. Conf.*, 1998, **36**, 259–274.
34. P. J. Jacques, E. Girault, T. Catlin, N. Geerlofs, T. Kop, S. van der Zwaag and F. Delannay: *Mater. Sci. Eng. A*, 1999, **A273–275**, 475–479.
35. P. J. Jacques, E. Girault, A. Martens, B. Verlinden, J. van Humbeeck and F. Delannay: *ISIJ Int.*, 2001, **41**, 1068–1074.
36. P. J. Jacques, Q. Furnemont, A. Mertens and F. Delannay: *Philos. Mag. A*, 2001, **81A**, 1789–1812.
37. S. J. Kim, C. G. Lee, I. Choi and S. Lee: *Metall. Mater. Trans. A*, 2001, **32A**, 505–514.
38. S. Traint, A. Pichler, R. Tikal, P. Stiaszny and E. Werner: *ISS Mech. Work. Steel Process. Proc. Conf.*, 2002, **40**, 39–152.
39. S. J. Kim, C. G. Lee, T. H. Lee and C. S. Oh: *ISIJ Int.*, 2002, **42**, 1452–1456.
40. C. G. Lee, S. J. Kim, C. S. Oh and S. Lee: *ISIJ Int.*, 2002, **42**, 1162–1168.
41. T. Nakagaito, T. Shimizu, O. Furukimi and K. Sakata: *Tetsu-to-Hagane*, 2003, **89**, 841–847.
42. S. Chatterjee: 'TRIP-assisted steels', PhD thesis, University of Cambridge, Cambridge, UK, 2006.
43. University of Cambridge and NPL: Materials Algorithms Project.
44. M. Murugananth, S. S. Babu and S. A. David: *Weld. J. (Res. Suppl.)*, 2004, **85**, 267s–276s.
45. 'Epogy 2003', Atlanta, GA, Synaps Inc., 2003.
46. MT-DATA Software, National Physical Laboratory, Teddington, UK, 2006.
47. H. K. D. H. Bhadeshia: *Met. Sci.*, 1981, **15**, 175–177.
48. H. K. D. H. Bhadeshia: *Met. Sci.*, 1981, **15**, 178–150.
49. H. K. D. H. Bhadeshia: *Acta Metall.*, 1981, **29**, 1117–1130.
50. H. K. D. H. Bhadeshia: *Met. Sci.*, 1982, **16**, 159–165.
51. D. B. Wiles and R. A. Young: *J. Appl. Crystallogr.*, 1981, **14**, 149–151.
52. T. Maki and C. M. Wayman: *Acta Metall.*, 1977, **25**, 681–693.
53. D. J. Dyson and B. Holmes: *J. Iron Steel Inst.*, 1970, **208**, 469–474.
54. H. K. D. H. Bhadeshia: *Mater. Sci. Eng. A*, 2007, to be published.